nature structural & molecular biology

Dxo1 is a new type of eukaryotic enzyme with both decapping and 5′-3′ exoribonuclease activity

Jeong Ho Chang[1,3], Xinfu Jiao[2,3], Kunitoshi Chiba[1], ChanSeok Oh[2], Charles E Martin[2], Megerditch Kiledjian[2] & Liang Tong[1]

Recent studies showed that Rai1 is a crucial component of the mRNA 5′-end-capping quality-control mechanism in yeast. The yeast genome encodes a weak homolog of Rai1, Ydr370C, but little is known about this protein. Here we report the crystal structures of Ydr370C from *Kluyveromyces lactis* and the first biochemical and functional studies on this protein. The overall structure of Ydr370C is similar to Rai1. Ydr370C has robust decapping activity on RNAs with unmethylated caps, but it has no detectable pyrophosphohydrolase activity. Unexpectedly, Ydr370C also possesses distributive, 5′-3′ exoRNase activity, and we propose the name Dxo1 for this new eukaryotic enzyme with both decapping and exonuclease activities. Studies of yeast in which both *Dxo1* and *Rai1* are disrupted reveal that mRNAs with incomplete caps are produced even under normal growth conditions, in sharp contrast to current understanding of the capping process.

The 5′ ends of messenger RNAs are rapidly capped during transcription in eukaryotes. The cap structure is crucial for the stability and translational efficiency of mRNAs[1–4]. Its removal is a highly regulated process that leads to mRNA degradation[5–9]. The 5′-end triphosphate group of the primary transcript is converted into the mature cap through three reactions and two intermediates. First, a 5′-end diphosphate group is generated by a triphosphatase. Then, a cap is produced by a guanylyltransferase through the attachment of GMP in a 5′-5′ linkage. Finally, the mature cap, m^7GpppN, is produced by a methyltransferase through methylation of the N^7 atom of the G base.

The capping process was generally believed to always proceed to completion and be devoid of any quality-control mechanism to maintain the fidelity of the 5′-end cap. However, if defects in 5′-end capping are present, the two intermediates as well as the primary transcript cannot be degraded by 5′-3′ exoRNases, because these enzymes prefer RNAs with 5′-end monophosphate[10–12]. These RNA species could not serve as substrates for the classical decapping enzymes either, as Dcp2 and Nudt16 are specific for the mature, methylated cap[5,7,9,13]. Therefore, separate enzymatic activities would be needed to degrade these intermediates that could accumulate if there were defects in 5′-end capping.

We recently reported that the yeast protein Rai1 has RNA 5′-end pyrophosphohydrolase (PPH) activity, removing a pyrophosphate from RNAs with 5′-end triphosphates[14]. Rai1 also has a newly identified decapping activity, being able to remove the entire cap (GpppN) from capped but unmethylated RNA, whereas its activity toward the mature cap is much lower[15]. This decapping activity is therefore highly distinct from that of Dcp2 and Nudt16, which produce m^7GDP (m^7Gpp) from the mature cap[5,7,9,13]. The observed biochemical activities of Rai1 suggest that it may be involved in RNA 5′-end-capping quality surveillance[14]. Studies in yeast have confirmed the existence of this new mechanism, showing that Rai1 is required for the degradation of RNAs with incomplete caps, especially under nutritional stress[15].

Rai1 is a single-copy gene in most organisms, and its mammalian homolog is known as Dom3Z[16]. However, the yeast *Saccharomyces cerevisiae* contains a homolog of Rai1, known by its systematic name Ydr370C[16]. The sequence conservation between Ydr370C and Rai1 is rather low, with roughly 20% amino acid identity, although residues that are important for catalysis are conserved (**Fig. 1**). Whereas Rai1 is in the nucleus, a global GFP-fusion-protein screen indicates that Ydr370C is in the cytoplasm[17], suggesting that each protein may have a distinct role in the cell. However, other than this general information, nothing is known about Ydr370C, and no detailed studies have been carried out on this protein, to our knowledge. We set out to determine the structure of Ydr370C and to assess whether it has similar biochemical and functional properties as Rai1.

We report here the crystal structures at up to 2.4-Å resolution of *K. lactis* Ydr370C alone and in complex with Mn^{2+} and demonstrate that Ydr370C possesses decapping activity on both capped but unmethylated and mature capped RNAs. In contrast to Rai1, Ydr370C does not possess PPH activity. Unexpectedly, our biochemical studies show that Ydr370C also has distributive, 5′-3′ exoRNase activity. We have named this newly identified eukaryotic enzyme Dxo1, as it carries both decapping and exoRNase activities. Our functional studies demonstrate that incomplete 5′-end capping occurs in yeast even under normal growth conditions, indicating the importance of 5′-end capping quality control.

[1]Department of Biological Sciences, Columbia University, New York, New York, USA. [2]Department of Cell Biology and Neuroscience, Rutgers University, Piscataway, New Jersey, USA. [3]These authors contributed equally to this work. Correspondence should be addressed to L.T. (ltong@columbia.edu) or M.K. (kiledjian@biology.rutgers.edu).

Received 1 February; accepted 2 August; published online 9 September 2012; doi:10.1038/nsmb.2381

Figure 1 Sequence conservation among Ydr370C (Dxo1), Rai1 and Dom3Z. Structure-based sequence alignment of *K. lactis* Ydr370C, *Schizosaccharomyces pombe* Rai1 and mouse Dom3Z. The secondary-structure elements (S. S.) in the Ydr370C structure are shown, and the four conserved sequence motifs are shown in red and labeled. Residues in Rai1 and Dom3Z that are located within 3 Å of the equivalent residue in Ydr370C are shown in uppercase. Residues that are disordered in the structures are shown in italic in lowercase. Black dots above the sequences indicate every tenth residue in the sequence of Ydr370C.

RESULTS

The structure of Ydr370C (Dxo1)

We determined the crystal structures of the *K. lactis* Ydr370C free enzyme and the Mn^{2+} complex at up to 2.4-Å resolution (**Fig. 2a** and **Table 1**). The overall structure of Ydr370C is similar to that of Rai1 and Dom3Z (**Supplementary Fig. 1**)[14], with r.m.s. distance of ~1.4 Å among equivalent Cα atoms. There are, however, clearly recognizable differences between these structures, including the positions of some of the β-strands and α-helices and the conformations of many of the surface loops (**Supplementary Fig. 1**). In addition, there are important amino acid variations in the active site region between Ydr370C and these other related enzymes (discussed below).

The structure of Ydr370C contains two mixed β-sheets, with 10 and 5 strands each, that are surrounded by 7 helices (**Fig. 2a**). Both β-sheets are highly twisted, and this is especially pronounced for the large β-sheet, as it has two separate concave faces. Helices αA and αH interact with these two concave faces, and helix αD interacts with the concave face of the small β-sheet. Helix αF is located between the two β-sheets and has interactions with both of them as well as with helices αB and αH. Two additional helices, α1 and α2, are located on the concave face of the small β-sheet but are far away from the large β-sheet.

Several segments of Ydr370C are disordered in the current structures. These include residues 1–37 (N terminus), 126–134 (α2-αA connection), 196–211 (β7-αD connection) and 229–237 (αD-β9 connection). Notably, residues 229–237 contain the β8-αE segment of Rai1, which is important for interactions with Rat1 (ref. 14). Ydr370C has a 13-residue deletion compared to Rai1 in this segment, and the sequences of the two proteins are not conserved here (**Fig. 1**). Ydr370C does not interact with Rat1 or Xrn1 when the purified proteins are mixed, and it does not interact with Rai1 either, on the basis of gel-filtration experiments on the mixtures (data not shown).

The active site of Ydr370C (Dxo1)

The active site of Ydr370C is located at an interface between the two β-sheets (**Fig. 2a**). In fact, strand β10 (in the large β-sheet) is separated from strand β11 (in the small β-sheet) by a single residue, Asp262, and there is a nearly 90° change in the direction of the protein backbone between the two strands (**Fig. 2a**) because this residue assumes a helical rather than an extended conformation. Asp262 is conserved among these enzymes and is a ligand to the divalent metal ion.

Residues that are centrally located in the active site come from four sequence motifs that are conserved among Rai1, Dom3Z and Ydr370C homologs (**Figs. 1** and **2b**). Motif I, an arginine residue, corresponds to Arg162 in *K. lactis* Ydr370C (at the beginning of helix αB; **Fig. 2b**). Motif II, GΦXΦE (where Φ is an aromatic or hydrophobic residue and X is any residue), corresponds to Gly219-Phe-Ala-Leu-Glu223 in Ydr370C (in helix αD). Motif III, EhD (where h is a hydrophobic residue), corresponds to Glu260-Met-Asp262 in Ydr370C (end of strand β10). Motif IV, EhK, corresponds to Glu273-Ile-Lys275 in Ydr370C (in strand β12).

In the structure of the Mn^{2+} complex, the metal ion is coordinated by the side chains of the glutamate residue in motif II (Glu223), the aspartate residue in motif III (Asp262) and the glutamate residue in motif IV (Glu273) (**Fig. 2b**). The main chain carbonyl oxygen of the hydrophobic residue of motif IV and two water molecules complete the octahedral coordination of the metal ion. This binding mode is similar to that observed in Rai1 (ref. 14). In the structure of the Ydr370C free enzyme, the side chain of Glu273 (motif IV) has a different conformation and is ion paired with that of Arg162 (motif I; **Fig. 2c**). In addition, a citrate molecule is bound in the active site in the structure of the free enzyme, and it occupies the position of the phosphate groups of GDP in the complex with Dom3Z (**Fig. 2c**)[14], consistent with the highly negative nature of the citrate molecule. However, the overall structures of the free enzyme and Mn^{2+} complex are highly similar to each other, with a r.m.s. distance of 0.3 Å for their Cα atoms.

Other residues in the active site region of Ydr370C include Leu161 (just before motif I, end of strand β5), His163 (just after motif I) and Asp167 from helix αB, and Lys290, Arg293 and Gln297 from helix αF (**Fig. 2b**). The three residues from helix αF are generally conserved in Rai1 and Dom3Z as well (**Fig. 1**), which suggests that they may be involved in substrate binding and/or catalysis. In comparison, the three other residues, Leu161, His163 and Asp167, are not conserved in Ydr370C homologs, but they are generally conserved as Trp/Phe/Tyr, Gly and Lys, respectively, in both Rai1 and Dom3Z (**Fig. 1**). Our biochemical studies show that variations at these three positions have important effects on the enzymatic activities of Ydr370C (discussed below).

The active site is defined by a deep pocket in the structures of Rai1 and Dom3Z[14]. In Ydr370C, owing to the disorder of two loops that form one wall of this pocket, residues 126–134 (α2-αA connection) and 196–211 (β7-αD connection), the active site appears to be more open (**Fig. 2d**). It may be expected that substrate binding can stabilize these loops and lead to a more defined active site pocket in Ydr370C.

Remote structural relationship to D-(D/E)XK nucleases

The structures of Rai1, Dom3Z and Ydr370C have a remote relationship to that of D-(D/E)XK nucleases[18], although little sequence conservation can be recognized with these enzymes. This relationship is primarily limited to the positions of the aspartate residue of motif III (EhD) and the entire motif IV (EhK) (**Fig. 3a**), which share a common

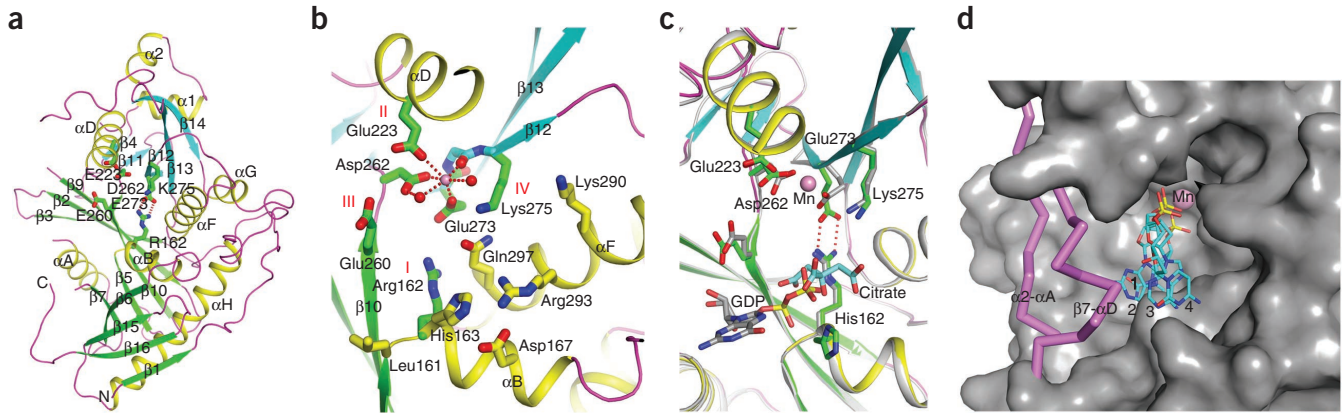

Figure 2 Crystal structures of Ydr370C (Dxo1). (**a**) Schematic drawing of the crystal structure of the *K. lactis* Ydr370C free enzyme. Strands in the two β-sheets are colored in cyan and green, respectively. The conserved motifs in the active site are shown as stick models, with carbon atoms in green. Red dashed lines indicate the bidentate ion-pair interactions between Arg162 and Glu273. (**b**) Structure of the active site region of *K. lactis* Ydr370C in complex with Mn^{2+}. Side chains from the four conserved motifs are colored green, and other side chains are in yellow. Mn^{2+} is shown as a pink sphere and two waters associated with it as red spheres. (**c**) Conformational differences in the active site region of Ydr370C between the free enzyme (in color) and the Mn^{2+} complex (in gray). A citrate molecule is bound in the free enzyme (cyan), and the position of GDP in the complex with Dom3Z[14] is also shown. (**d**) Molecular surface of Ydr370C in the active site region. The Mn^{2+} ion is shown as a pink sphere and labeled. The α2-αA and β7-αD connections in the structure of *S. pombe* Rai1 (ref. 14) are shown for reference (in violet). A single-stranded nucleic acid (four nucleotides, labeled) was positioned in the active site pocket (in cyan) on the basis of the structure of the HincII endonuclease in complex with substrate[25]. All the structure figures were produced with PyMOL (www.pymol.org).

role in binding the metal ion in all of these enzymes. The related enzymes include herpesvirus and baculovirus nucleases (**Fig. 3b**)[19,20], with a *Z* score of 4.8 and 9% sequence identity to Ydr370C (on the basis of DaliLite[21]), *Escherichia coli* prophage RecE 5′-3′ exonuclease (*Z* score 5.2, 10% identity) (**Fig. 3c**)[22], λ phage 5′-3′ exonuclease (*Z* score of 5.1, 9% identity) (**Fig. 3d**)[23] and type II restriction endonucleases[24], including HincII (*Z* score 3.6, 8% identity) (**Fig. 3e**)[25], EcoRV, EcoRI, BamHI, BglI and others. Outside of these two motifs, the structural conservation among these enzymes is much lower.

Stronger structural similarity is observed with the viral and (pro)phage nucleases. The central core of these structures includes a three-stranded β-sheet (corresponding to strands β5, β9 and β10 in the large β-sheet of Ydr370C) and another β-sheet with five or more strands (the small β-sheet of Ydr370C). In addition, helices αB, αD, αF and αH in Ydr370C have equivalents in these D-(D/E)XK nucleases. However, Rai1, Dom3Z and Ydr370C also contain additional unique conserved motifs. The aspartate is part of the EhD motif, and the glutamate residue is not present in these other enzymes. The arginine residue of motif I is also unique to Rai1, Dom3Z and Ydr370C. The glutamate residue of motif II, GΦXΦE, is present in herpesvirus nuclease and the λ phage nuclease but is absent in the other D-(D/E)XK enzymes.

In contrast, structural similarity with the type II restriction enzymes is much weaker. The three-stranded β-sheet and helices αB and αF are absent in these structures (**Fig. 3e**). As a result, the active site region of these enzymes is much more open, which may be consistent with their endonuclease activity on double-stranded DNA substrates.

Ydr370C (Dxo1) has strong decapping activity but no PPH activity

We next tested whether Ydr370C has biochemical activities similar to those of Rai1. As expected, Ydr370C demonstrated robust decapping activity toward capped but unmethylated RNA, and it released GpppG as the product (**Fig. 4a**). However, in contrast to Rai1, Ydr370C did not show PPH activity toward an RNA substrate with 5′-end triphosphate (**Fig. 4b**). Moreover, whereas Rai1 possesses weak hydrolytic activity on mature, methylated caps[15], Ydr370C exhibited appreciable decapping activity toward this substrate, releasing the m^7GpppG cap structure, albeit at a lower efficiency than the unmethylated capped substrate (**Fig. 4a**). Neither decapping activity of Ydr370C was stimulated by Rat1 or Xrn1 (**Fig. 4a**), consistent with the lack of interactions between these proteins.

Table 1 Data collection and refinement statistics

	Free enzyme	Mn^{2+} complex
Data collection		
Space group	$P6_122$	$P6_122$
Cell dimensions		
a, *b*, *c* (Å)	82.82, 82.82, 259.85	82.13, 82.13, 260.73
α, *β*, *γ* (°)	90, 90, 120	90, 90, 120
Resolution (Å)[a]	30–2.4 (2.49–2.4)	30–2.8 (2.90–2.8)
R_{merge} (%)	7.3 (40.8)	6.1 (45.5)
$I / \sigma I$	20.6 (3.0)	24.9 (4.8)
Completeness (%)	96 (75)	99 (100)
Redundancy	6.4 (5.1)	6.7 (7.0)
Refinement		
Resolution (Å)	30–2.4	30–2.8
No. reflections	20,135	12,851
R_{work} / R_{free} (%)	19.7 / 24.0	20.2 / 25.7
No. atoms		
Protein	2,692	2,692
Ligand/Ion	13	1
Water	148	49
B-factors		
Protein	53.3	78.6
Ligand/Ion	84.8	74.2
Water	57.2	64.8
R.m.s. deviations		
Bond lengths (Å)	0.013	0.012
Bond angles (°)	1.7	1.6

[a]The numbers in parentheses are for the highest-resolution shell. One crystal was used for each data collection.

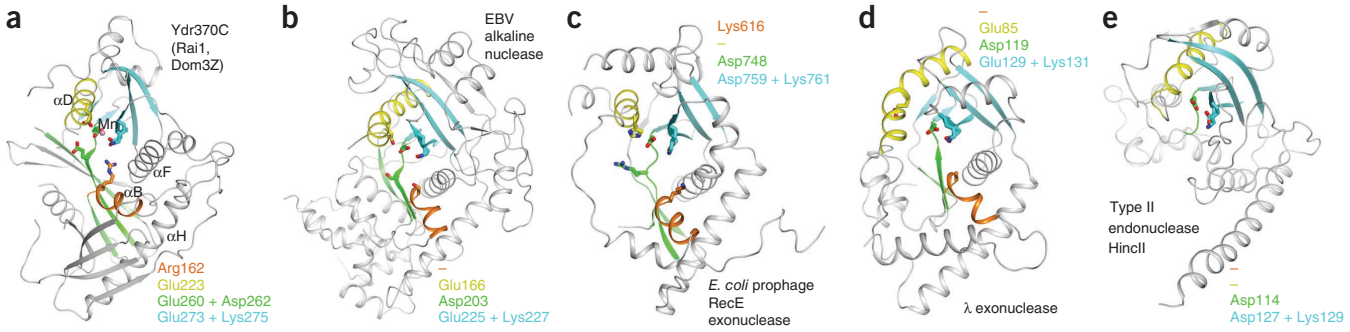

Figure 3 Remote structural similarity to D-(D/E)XK nucleases. (**a**) Schematic drawing of the structure of Ydr370C. Motif I and helix αB are shown in orange, motif II and helix αD in yellow, motif III and its associated β-strands in green, motif IV and its associated β-strands in cyan. The Mn^{2+} ion is shown as a sphere in pink. (**b**) Structure of herpesvirus alkaline nuclease[19,20], in the same view as that for Ydr370C in **a**. (**c**) Structure of *E. coli* prophage RecE 5′-3′ exonuclease[22]. (**d**) Structure of λ phage 5′-3′ exonuclease[23]. (**e**) Structure of type II restriction endonuclease HincII[25]. Residues in the four conserved motifs of Ydr370C and their equivalents in the other enzymes are indicated in each of the panels. A dash means that a functionally equivalent residue is absent.

We introduced mutations in the putative active site region and assessed their effects on the decapping and PPH activities of Ydr370C. Mutation of residues in conserved motif III (E260A, D262A, and E260A D262A) abrogated the decapping activity (**Fig. 4c**). Notably, the E260A and D262A single-site mutants were able to release a small amount of m^7Gpp (**Fig. 4c**) in a manner similar to the activity of classical decapping enzymes. We also converted the three residues unique to Ydr370C in the active site region to their equivalents in Rai1 and Dom3Z —L161W, H163G and D167K single-site mutants as well as L161W H163G and H163G D167K double mutants. The L161W H163G D167K triple mutant was also generated, but the protein became insoluble during *E. coli* expression.

The L161W and L161W H163G mutants had reduced decapping activity, whereas the D167K mutant behaved like wild-type enzyme (**Fig. 4c**). All of these mutants, with the exception of D167K, also released a small amount of m^7Gpp. Unexpectedly, the H163G and H163G D167K mutants also exhibited substantial activity toward an RNA substrate with 5′-end triphosphate, and the D167K mutant showed weak activity toward this substrate (**Fig. 4d**). Careful analysis showed, however, that the released product is not pyrophosphate (**Fig. 4d**) but rather GTP (Gppp) (**Fig. 4e**), suggesting an activity that is somewhat similar to the decapping activity of Ydr370C. Overall, these data indicate the importance of Leu161, His163 and Asp167 in the activity of Ydr370C and suggest that Ydr370C may function as a decapping enzyme in cells.

Ydr370C (Dxo1) has distributive 5′-3′ exoRNase activity

Unexpectedly, throughout the course of these studies, we observed evidence in our assays that Ydr370C also possessed 5′-3′ exoRNase activity. With an RNA substrate labeled at the 5′ end with [^{32}P]phosphate,

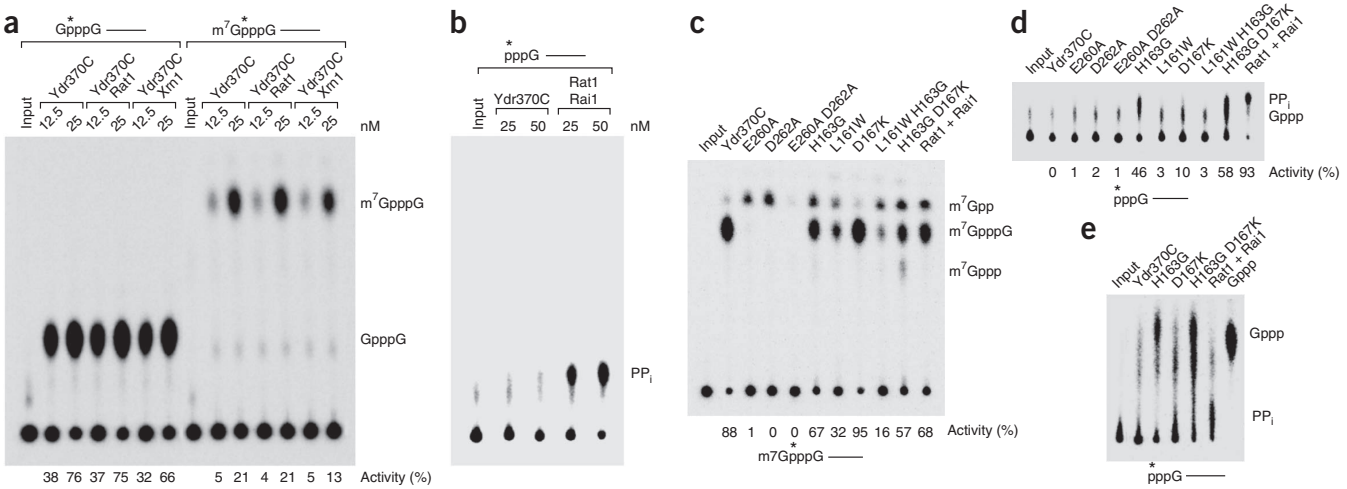

Figure 4 Ydr370C (Dxo1) has strong decapping activity but no PPH activity. (**a**) Decapping assay monitored by thin-layer chromatography (TLC). Decapping activity of Ydr370C toward capped but unmethylated and mature, methylated RNA. The percentage of substrate turnover is indicated at the bottom. Rat1 and Xrn1 have no effect on the decapping activity. A schematic of the RNA used is indicated at the top, with the asterisks denoting the position of the ^{32}P labeling. (**b**) PPH assay monitored by TLC. Ydr370C had essentially no PPH activity under the assay condition tested. Rai1 was used as a positive control. (**c**) The effects of mutations in the active site region on the decapping activity of Ydr370C. Most of the mutants were also able to release small amounts of a new product, m^7Gpp. (**d**) PPH assay monitored by TLC. The H163G, H163G D167K and D167K mutations in the active site region confer activity toward an RNA with 5′-end triphosphate. (**e**) The product released by the H163G, H163G D167K and D167K mutants from an RNA with 5′-end triphosphate is GTP (Gppp) rather than pyrophosphate (PP_i). A different running buffer was used to more clearly separate PP_i from Gppp. Gppp in the sample lanes migrates slightly differently compared to the marker, as the samples are in a buffer and also contain protein, whereas the marker is in water.

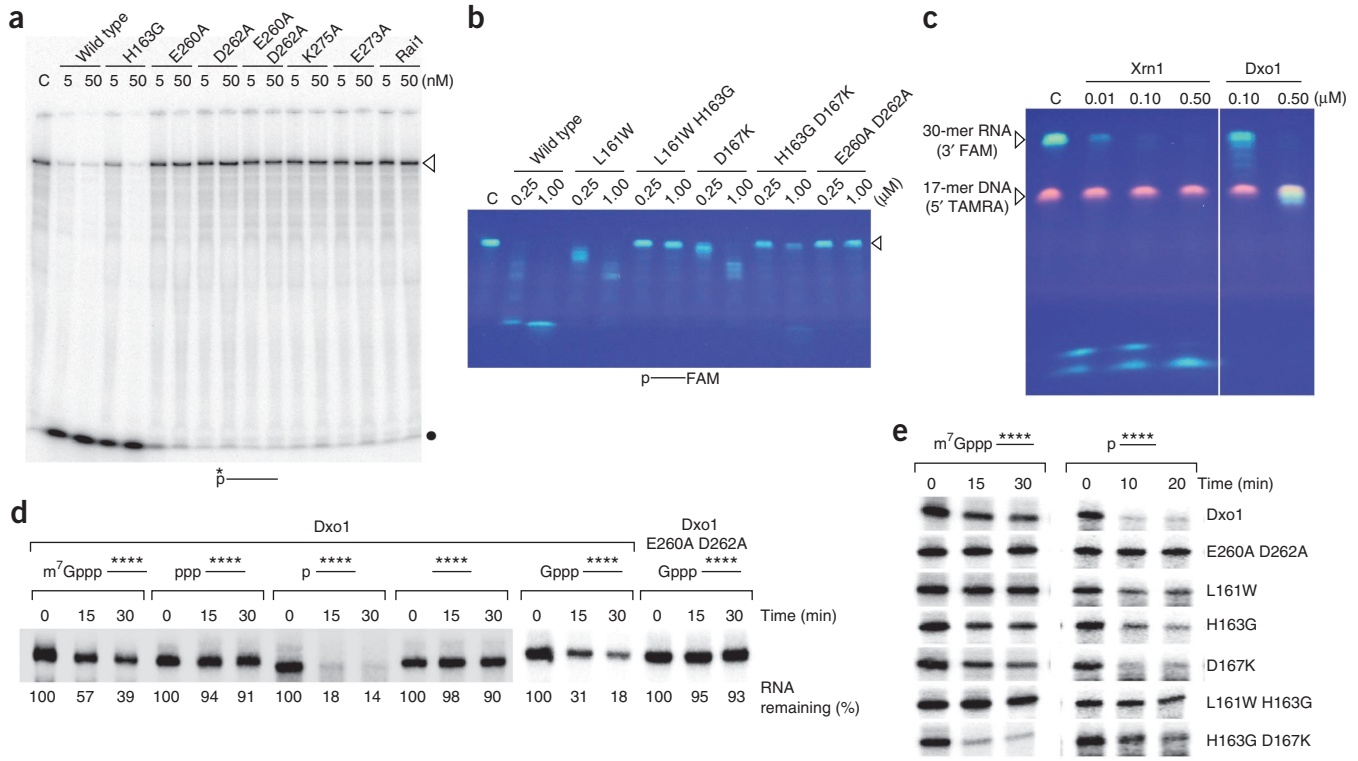

Figure 5 Ydr370C (Dxo1) has distributive 5′-3′ exoRNase activity. (**a**) Activity of wild-type Ydr370C and various mutants toward a 240-nucleotide RNA substrate labeled at the 5′ end (as denoted by the asterisk). The position of unreacted, full-length substrate is marked with the arrowhead, and the dot indicates the migration of single nucleotides at the front of the gel. C, no-enzyme control. (**b**) Activity of Ydr370C toward a 30-nucleotide RNA substrate with 5′-end monophosphate and 3′-end FAM fluorophore label, confirming the distributive 5′-3′ exonuclease activity. (**c**) Activity of Ydr370C toward an RNA-DNA heteroduplex substrate[26]. *K. lactis* Xrn1 (residues 1–1,245)[27] was included as a comparison. (**d**) Activity of Ydr370C (Dxo1) on a panel of RNAs uniformly labeled with ^{32}P (denoted by a line with multiple asterisks) and with different 5′-end modifications. The E260A D262A mutant was used as a negative control. (**e**) Activity of wild-type Ydr370C (Dxo1) and mutants toward body-labeled RNA with 5′-end methylated cap or monophosphate.

Ydr370C readily released the labeled mononucleotide, and no other intermediates were observed (**Fig. 5a**), which suggested a 5′-3′ exoRNase activity. In contrast, Rai1 showed no nuclease activity toward this substrate (**Fig. 5a**), consistent with earlier data[16]. We next used a 30-mer RNA substrate with a 5′-end monophosphate and labeled at the 3′ end with the FAM (6-carboxyfluorescein) fluorophore[26]. Cleavage intermediates were observed during the reaction, ultimately leading to the production of the labeled 3′-end nucleotide (**Fig. 5b**). However, the equivalent single-stranded DNA (ssDNA) substrate was essentially not degraded (**Supplementary Fig. 2**). Gel-shift experiments demonstrated the binding of both RNA and ssDNA to Ydr370C (**Supplementary Fig. 3**). Gpp and GpppG do not compete against the decapping reaction (**Supplementary Fig. 3**), which suggests that they may have a relatively low affinity for the active site.

Mutations in the conserved motifs III and IV of Ydr370C abolished the exonuclease activity (**Fig. 5a**). The L161W, H163G and D167K single-site mutants showed good nuclease activity, whereas the L161W H163G and H163G D167K double mutants had much lower activity (**Fig. 5a**,**b**). Overall, our biochemical data demonstrate that Ydr370C possesses both decapping and distributive 5′-3′ exoRNase activities. Such an enzyme has not been described previously, and we propose the name Dxo1 for this protein and will refer to Ydr370C by this name from here on.

To further characterize the exoRNase activity of Dxo1, we used an RNA-DNA heteroduplex substrate that was developed for assaying 5′-3′ exoRNases[26]. The 30-mer FAM-labeled RNA strand is the same as the one described above (**Fig. 5b**). The 17-mer DNA strand has a 5′-end tetramethylrhodamine (TAMRA) label and anneals to the 3′ end of the RNA strand, predominantly AT base pairs. Our nuclease assays showed that Dxo1 was able to degrade the 13-nucleotide RNA overhang at the 5′ end but was then stalled at the duplex portion of the substrate (**Fig. 5c**). In contrast, Xrn1 efficiently degraded the entire RNA strand. Overall, it appears that Dxo1 is a weaker 5′-3′ exoRNase than Xrn1 and is more prone to stalling due to secondary-structure elements in the substrate.

To determine whether there is a correlation between the exoRNase and the decapping activities, we assayed Dxo1 against a panel of substrates with the same RNA body but different 5′-end modifications (**Fig. 5d**). RNAs with a 5′-end monophosphate, unmethylated cap, or methylated cap were degraded, whereas those with a 5′-end triphosphate or hydroxyl group were not. Therefore, the exonuclease activity requires prior decapping and generation of a 5′-end monophosphate for capped RNAs. RNA with 5′-end triphosphate is a poor substrate because Dxo1 does not have PPH activity. The more efficient degradation of the 5′-end monophosphate RNA relative to the capped RNAs indicates that the decapping step rather than the exonuclease step may be rate limiting. Assays with Dxo1 mutants confirmed the observations with the wild-type enzyme (**Fig. 5e**), except for the H163G D167K double mutant, for which we consistently observed more efficient activity on methylated capped RNA. At present, it is not obvious how this particular double mutant more efficiently couples the decapping and exonuclease activities.

Incomplete 5′-end capping under normal growth conditions

To characterize the physiological function of Dxo1, we examined the steady-state levels of three representative mRNAs, PGK1, ACT1 and

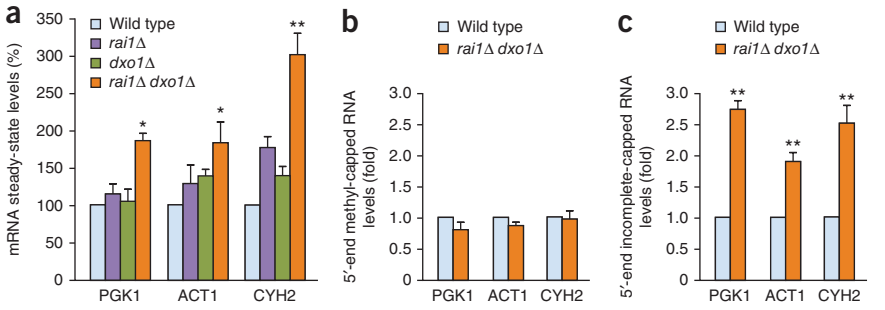

Figure 6 Dxo1 is involved in mRNA 5′-end capping quality control. (**a**) Real-time reverse-transcription PCR (RT-PCR) quantitation of PGK1, ACT1 and CYH2 mRNAs. Levels of PGK1, ACT1 and CYH2 mRNAs in the various yeast cells under normal growth conditions are shown. Data are presented relative to the 18S rRNA, with the level of mRNA in wild-type cells set to 100. A significant increase in steady-state mRNA levels was observed in the *rai1Δ dxo1Δ* doubly disrupted strain for all three mRNAs. Error bars indicate s.d. from three independent experiments. (**b**) Levels of methylated capped RNAs, immunoprecipitated using monoclonal anti-trimethylguanosine antibody column, are shown for the indicated yeast strains, normalized relative to the amount of total input RNA, with levels in the respective wild-type cells set to 1. (**c**) Levels of mRNA lacking a 5′-end methylated cap. Levels were normalized relative to 18S rRNA, and mRNA levels in wild-type cells were set to 1. Error bars indicate s.d. from six independent experiments. *, $P < 0.01$; **, $P < 0.001$. The *P* values were determined with Student's *t*-test.

CYH2, in yeast cells under normal growth conditions. Disruption of *Dxo1* or *Rai1* alone had little effect on the levels of these mRNAs (**Fig. 6a**), suggesting that, similar to Rai1, Dxo1 is not a general mRNA decapping enzyme and, in cells, may function predominantly on RNAs with incomplete caps.

Unexpectedly, significant increases in levels of all three mRNAs were detected in the *rai1Δ dxo1Δ* doubly disrupted strain relative to 18S rRNA (**Fig. 6a**). To determine whether the increases in mRNA levels were due to methylated capped mRNA or incompletely capped mRNA, the two species of mRNAs were separated with an anti-cap antibody affinity column under conditions that resolve methylated capped mRNAs from defectively capped mRNAs containing an unmethylated cap or no cap (pppRNA) (**Supplementary Fig. 4**). Notably, differences in levels of methylated capped mRNA were not detected between wild-type and *rai1Δ dxo1Δ* double-mutant strains (**Fig. 6b**), whereas a significant increase in incompletely capped or uncapped mRNAs was detected in the double mutant compared to wild type for all three mRNAs tested (**Fig. 6c**). These data demonstrate that the levels of incompletely capped but not normally capped mRNAs are responsive to Rai1 and Dxo1.

To exclude the possibility that the RNAs with defective 5′-end capping are actually decapped decay intermediates (with 5′-end monophosphate), we first treated these RNAs with the 5′-3′ exoRNase Xrn1 from *K. lactis*[27], which has strong processive activity toward RNA with 5′-end monophosphate, under conditions that greatly reduced the levels of the input rRNA (**Supplementary Fig. 5**). No differences were observed with the methyl-capped mRNAs tested between wild-type and *rai1Δ dxo1Δ* double mutant strains (**Supplementary Fig. 5**). Consistent with the results obtained with the samples not treated with Xrn1, approximately twice as much incompletely capped mRNAs was still evident in the double-disrupted strain relative to the wild-type strain for all three mRNAs tested (**Supplementary Fig. 5**). However, as expected, a modest reduction in the levels of the defective mRNAs was observed, likely attributable to decay intermediates that accumulate because of reduced Rat1 activity in the absence of the Rai1 stimulatory function and the absence of Dxo1 exoRNase activity.

To assess the cellular compartment(s) in which Dxo1 may be functioning, we localized tandem-affinity purification (TAP)–tagged Dxo1 by confocal microscopy and found that Dxo1 is primarily in the cytoplasm (**Supplementary Fig. 6**), consistent with a previous report based on a genome-wide screen[17]. In addition, we found that Dxo1 also resides in the nucleus. Therefore, Rai1 appears to fulfill a nuclear quality-control mechanism to clear incompletely capped mRNAs, whereas Dxo1 could fulfill a complementary function in the nucleus as well as in the cytoplasm, on mRNAs that have escaped the nucleus, to clear these potentially deleterious molecules from the cell.

DISCUSSION

Although the overall structures of Dxo1, Rai1 and Dom3Z are similar, these three enzymes have distinct biochemical properties. For example, Rai1 possesses PPH activity and is selective toward the unmethylated cap, whereas Dxo1 does not have PPH activity but shows appreciable activity toward the methylated cap. In addition, Dxo1 possesses 5′-3′ exonuclease activity, but Rai1 does not. Moreover, the H163G and H163G D167K mutants of Dxo1 acquired catalytic activity toward 5′-end triphosphorylated RNA, but the released product is Gppp (GTP) rather than PP_i (**Fig. 4e**). Variations in the active site region between Dxo1 and Rai1, as well as the mutations introduced into the active site region of Dxo1 for these studies, may have affected the detailed placement of the substrates, giving rise to the different catalytic activities and the product profiles for Dxo1, its mutants and Rai1. On the basis of the structure of HincII in complex with a double-stranded DNA substrate[25], we built a model for the possible position of the nucleic acid substrate in the active site pocket of Dxo1 (**Fig. 2d**). Only a single-stranded structure (with four nucleotides) can be accommodated in this pocket, consistent with our biochemical observations (**Fig. 5c**). At the same time, this model does not provide insights into the catalytic mechanism of Dxo1, which will require crystal structures on the substrate complexes of this enzyme. Our inability to separate the decapping and exonuclease activities with the different Dxo1 mutants tested suggests that the different activities may use the same active site.

The structural similarity between Dxo1, Rai1, Dom3Z and the viral nucleases suggests a viral origin for these cellular enzymes. Dxo1, Rai1 and Dom3Z do not appear, on the basis of amino acid sequence analysis, to have other cellular homologs, and their structural similarity to the type II restriction enzymes is much more limited than their similarity to the viral nucleases (**Fig. 3**). At the same time, Dxo1, Rai1 and Dom3Z have also diverged substantially from these potential viral ancestors, acquiring extra conserved sequence motifs and structural features, which endow these enzymes with the decapping and PPH catalytic activities. Especially, the presence of an additional acidic residue in motif III (EhD) is a distinguishing feature for Dxo1, Rai1 and Dom3Z, which may play an important part in the unique catalytic activities of these enzymes. It is probably unlikely that the viral nucleases also possess decapping and/or PPH activity.

The functional data demonstrate that incompletely capped mRNAs are produced in yeast cells even under normal growth conditions, and the extent of incompletely capped mRNA approximately

doubles in the absence of Rai1 and Dxo1. These findings extend our earlier studies that revealed the presence of defectively capped mRNA under stress conditions[15]. However, the possibility that the double knockout mimics a stress condition cannot be ruled out. Collectively, our results are in sharp contrast to the current understanding of the 5′-end capping process, which is based on the premise that capping always proceeds to completion and there are no defects with this process.

Overall, our biochemical and functional studies demonstrate that Ydr370C (Dxo1) is a newly identified eukaryotic enzyme with an important role in mRNA 5′-end capping quality surveillance, a function similar to that of Rai1. However, the slow-growth phenotype of the *rai1Δ* strain[16], which is not observed in the *dxo1Δ* strain (**Supplementary Fig. 6**), indicates that Dxo1 cannot rescue this defect, which suggests that Rai1 and Dxo1 should also have distinct functions and/or substrates in the cell. Some of these functions of Dxo1 may be mediated by its 5′-3′ exonuclease activity. In fact, Dxo1 is unique in that it can singlehandedly decap and degrade mRNAs, whereas Rai1 and the classical decapping enzymes (Dcp2, Nudt16) require 5′-3′ exoRNases (Rat1, Xrn1)[12,28–30] in order to completely degrade mRNAs. In addition, a class of Xrn1-sensitive noncoding RNAs (XUTs) has been reported recently[31], which includes a subset of cryptic unstable transcripts (CUTs)[32] and stable uncharacterized transcripts (SUTs) identified earlier. The degradation of these RNAs in the cytoplasm requires decapping, and whether Dxo1 also regulates these XUTs and/or functions on other RNAs remains to be determined.

METHODS

Methods and any associated references are available in the online version of the paper.

Accession codes. The atomic coordinates have been deposited at the Protein Data Bank, with accession codes 4GPS and 4GPU.

Note: Supplementary information is available in the online version of the paper.

ACKNOWLEDGMENTS

We thank T.G. Kinzy (University of Medicine and Dentistry of New Jersey, Piscataway , New Jersey, USA) for the TAP-tagged Ydr370C strain; N. Whalen, S. Myers and H. Robinson for setting up the X29A beamline at the National Synchrotron Light Source . This research was supported by grants from the US National Institutes of Health to L.T. (GM090059) and M.K. (GM67005).

AUTHOR CONTRIBUTIONS

J.H.C. and K.C. performed protein expression, purification and crystallization experiments. J.H.C. carried out crystallographic data collection, structure determination and refinement, as well as mutagenesis and exonuclease assays. X.J. carried out decapping assays and all the studies in yeast cells. C.O. and C.E.M. generated the *Rai1* and *Dxo1* deletion strains. All authors commented on the manuscript. L.T. and M.K. designed experiments, analyzed data, supervised the project and wrote the paper.

COMPETING FINANCIAL INTERESTS

The authors declare no competing financial interests.

Published online at http://www.nature.com/doifinder/10.1038/nsmb.2381.
Reprints and permissions information is available online at http://www.nature.com/reprints/index.html.

1. Shatkin, A.J. & Manley, J.L. The ends of the affair: capping and polyadenylation. *Nat. Struct. Biol.* **7**, 838–842 (2000).
2. Shuman, S. The mRNA capping apparatus as drug target and guide to eukaryotic phylogeny. *Cold Spring Harb. Symp. Quant. Biol.* **66**, 301–312 (2001).
3. Hocine, S., Singer, R.H. & Grunwald, D. RNA processing and export. *Cold Spring Harb. Perspect. Biol.* **2**, a000752 (2010).
4. Ghosh, A. & Lima, C.D. Enzymology of RNA cap synthesis. *Wiley Interdiscip. Rev. RNA* **1**, 152–172 (2010).
5. Coller, J. & Parker, R. Eukaryotic mRNA decapping. *Annu. Rev. Biochem.* **73**, 861–890 (2004).
6. Cougot, N., van Dijk, E., Babajko, S. & Seraphin, B. 'Cap-tabolism'. *Trends Biochem. Sci.* **29**, 436–444 (2004).
7. Franks, T.M. & Lykke-Andersen, S. The control of mRNA decapping and P-body formation. *Mol. Cell* **32**, 605–615 (2008).
8. Houseley, J. & Tollervey, D. The many pathways of RNA degradation. *Cell* **136**, 763–776 (2009).
9. Li, Y. & Kiledjian, M. Regulation of mRNA decapping. *Wiley Interdiscip. Rev. RNA* **1**, 253–265 (2010).
10. Stevens, A. An exoribonuclease from *Saccharomyces cerevisiae*: effect of modifications of 5′ end groups on the hydrolysis of substrates to 5′ mononucleotides. *Biochem. Biophys. Res. Commun.* **81**, 656–661 (1978).
11. Stevens, A. Purification and characterization of a *Saccharomyces cerevisiae* exoribonuclease which yields 5′-mononucleotides by a 5′→3′ mode of hydrolysis. *J. Biol. Chem.* **255**, 3080–3085 (1980).
12. Chang, J.H., Xiang, S. & Tong, L. 5′-3′ exoribonucleases. in *Ribonucleases, Nucleic Acids and Molecular Biology* Vol. 26 (ed. Nicholson, A.W.) Ch. 7, 167–192 (Springer, 2011).
13. Song, M.-G., Li, Y. & Kiledjian, M. Multiple mRNA decapping enzymes in mammalian cells. *Mol. Cell* **40**, 423–432 (2010).
14. Xiang, S. *et al.* Structure and function of the 5′→3′ exoribonuclease Rat1 and its activating partner Rai1. *Nature* **458**, 784–788 (2009).
15. Jiao, X. *et al.* Identification of a quality-control mechanism for mRNA 5′-end capping. *Nature* **467**, 608–611 (2010).
16. Xue, Y. *et al. Saccharomyces cerevisiae* RAI1 (YGL246c) is homologous to human DOM3Z and encodes a protein that binds the nuclear exoribonuclease Rat1p. *Mol. Cell. Biol.* **20**, 4006–4015 (2000).
17. Huh, W.K. *et al.* Global analysis of protein localization in budding yeast. *Nature* **425**, 686–691 (2003).
18. Aravind, L., Makarova, K.S. & Koonin, E.V. Holliday junction resolvases and related nucleases: identification of new families, phyletic distribution and evolutionary trajectories. *Nucleic Acids Res.* **28**, 3417–3432 (2000).
19. Buisson, M. *et al.* A bridge crosses the active-site canyon of the Epstein-Barr virus nuclease with DNase and RNase activities. *J. Mol. Biol.* **391**, 717–728 (2009).
20. Dahlroth, S.-L., Gurmu, D., Haas, J., Erlandsen, H. & Nordlund, P. Crystal structure of the shutoff and exonuclease protein from the oncogenic Kaposi's sarcoma-associated herpesvirus. *FEBS J.* **276**, 6636–6645 (2009).
21. Holm, L., Kaariainen, S., Rosenstrom, P. & Schenkel, A. Searching protein structure databases with DaliLite v.3. *Bioinformatics* **24**, 2780–2781 (2008).
22. Zhang, J., Xing, X., Herr, A.B. & Bell, C.E. Crystal structure of *E. coli* RecE protein reveals a toroidal tetramer for processing double-stranded DNA breaks. *Structure* **17**, 690–702 (2009).
23. Kovall, R. & Matthews, B.W. Toroidal structure of lambda-exonuclease. *Science* **277**, 1824–1827 (1997).
24. Kovall, R.A. & Matthews, B.W. Type II restriction endonucleases: structural, functional and evolutionary relationships. *Curr. Opin. Chem. Biol.* **3**, 578–583 (1999).
25. Joshi, H.K., Etzkorn, C., Chatwell, L., Bitinaite, J. & Horton, N.C. Alteration of sequence specificity of the type II restriction endonuclease HincII through an indirect readout mechanism. *J. Biol. Chem.* **281**, 23852–23869 (2006).
26. Sinturel, F. *et al.* Real-time fluorescence detection of exoribonucleases. *RNA* **15**, 2057–2062 (2009).
27. Chang, J.H., Xiang, S., Xiang, K., Manley, J.L. & Tong, L. Structural and biochemical studies of the 5′→3′ exoribonuclease Xrn1. *Nat. Struct. Mol. Biol.* **18**, 270–276 (2011).
28. Buratowski, S. Connections between mRNA 3′ end processing and transcription termination. *Curr. Opin. Cell Biol.* **17**, 257–261 (2005).
29. Conti, E. & Izaurralde, E. Nonsense-mediated mRNA decay: molecular insights and mechanistic variations across species. *Curr. Opin. Cell Biol.* **17**, 316–325 (2005).
30. Isken, O. & Maquat, L.E. Quality control of eukaryotic mRNA: safeguarding cells from abnormal mRNA function. *Genes Dev.* **21**, 1833–1856 (2007).
31. van Dijk, E.L. *et al.* XUTs are a class of Xrn1-sensitive antisense regulatory non-coding RNA in yeast. *Nature* **475**, 114–117 (2011).
32. Thompson, D.M. & Parker, R. Cytoplasmic decay of intergenic transcripts in *Saccharomyces cerevisiae*. *Mol. Cell. Biol.* **27**, 92–101 (2007).

ONLINE METHODS

Protein expression and purification. Full-length *K. lactis* Ydr370C was cloned into the pET28a vector (Novagen, with N-terminal His tag). The protein was overexpressed in *E. coli* BL21 Rosetta (DE3) cells at 20 °C. The cells were lysed by sonication, and the recombinant protein was purified by Ni-NTA (Qiagen) and gel-filtration (Sephacryl S-300, GE Healthcare) chromatography. Purified Ydr370C was concentrated to 10 mg/ml in a buffer containing 20 mM Tris, pH 7.5, 200 mM NaCl, 2 mM DTT and 5% (v/v) glycerol, flash frozen in liquid nitrogen and stored at −80 °C.

The selenomethionyl (SeMet) protein sample was produced in minimal medium supplemented with specific amino acids to inhibit endogenous methionine biosynthesis, and the bacteria were grown in the presence of selenomethionine[33]. The purification procedure is the same as that for the native protein, except that the DTT concentration in the storage buffer was increased to 10 mM.

Protein crystallization. Crystals were obtained with the sitting-drop vapor-diffusion method at 20 °C. The reservoir solution contained 200 mM sodium citrate tribasic and 23.5% (w/v) PEG 3350. Initial crystals of the SeMet protein were obtained by cross-seeding with crystals of the native protein. Crystals were flash frozen in liquid nitrogen for diffraction analysis and data collection at 100 K.

In attempts to observe binding of substrates to the active site, native crystals were first soaked in a solution containing 100 mM Tris, pH 7.5, 22% (w/v) PEG 4000 and 150 mM NaCl, to remove the citrate, and then soaked in solutions containing 100 mM Tris, pH 7.5, 22% (w/v) PEG 4000, 17% (v/v) glycerol, 50–150 mM NaCl, 10 mM Mn^{2+} and up to 30 mM of (oligo)nucleotides or cap analogs.

Data collection and structure determination. Native and multiwavelength anomalous diffraction data sets were collected at NSLS beamline X29A. The diffraction data were processed and scaled with the HKL package[34]. The crystals belong to space group $P6_122$, with cell parameters of $a = b = 83.2$ Å and $c = 259.8$ Å for the native crystal. There is one molecule of Ydr370C in the crystallographic asymmetric unit. The data processing statistics are summarized in **Table 1**.

The selenium atoms were located with the program BnP[35], and the reflections were phased with the program Solve[36]. Manual model building was performed with the program O[37] and Coot[38]. The structure refinement was carried out with the program CNS[39].

Mutagenesis. Site-specific mutations were created with the QuikChange kit (Stratagene), and sequencing was performed to confirm correct incorporation of the mutations. The mutant proteins were purified by Ni-NTA (Qiagen) and gel-filtration (Superose 12, GE Healthcare) chromatography.

Yeast strains. Genotypes of all the *S. cerevisiae* strains used in this study are listed in **Supplementary Table 1**. The *ABD WT* control and *rai1* gene disruption (*ABD1; rai1Δ*) strains have been reported[15,40]. To assemble the *YDR370C* gene-disruption construct, the 5′ and 3′ untranslated region (UTR) of *YDR370C* were individually isolated from the chromosomal DNA of DTY-10A by using the PCR primer pairs YDR5F and YDR5R for the 5′ UTR and YDR3F and YDR3R for the 3′ UTR. Amplified fragments were ligated into the vector pBlu2-HIS3 to create pBlue(HIS3)-Y5 and pBlue(HIS3)-Y3. The pBlue-Δydr370c::HIS3 construct for generating the *YDR370C* gene disruption strain was generated by ligation of the XhoI-ClaI fragment of pBlue(HIS3)-Y5 into the corresponding sites of pBlue(HIS3)-Y3. The chromosomal *YDR370C* gene was disrupted by transformation of the *ABD1 WT* and *ABD1; rai1Δ* strains with a DNA fragment isolated from the vector by double digestion with restriction enzymes XbaI and XhoI. The transformants were selected on His(−)-glucose plates. Strains were transformed with the disrupted forms of DNA fragments encoding the *YDR370C* gene by using the BD Biosciences Yeastmaker Transformation System 2 method. The correct transformants were screened by PCR primer pairs, Con-Y5F + Con-H3Rev and Con-H3For + Con-Y3R. The sequences of the primers are listed in **Supplementary Table 2**.

Yeast growth condition and RNA isolation. All wild-type and mutant strains were grown in normal medium at 30 °C till mid log phase, and then the cells were harvested and total RNAs were isolated with the acidic hot-phenol method as described[41].

RNA generation and *in vitro* decay assays. The 5′-end radiolabeled RNA substrate for **Figure 5a** was prepared as described previously[27]. The fluorescently labeled RNA and DNA oligonucleotides[26] were purchased from Integrated DNA Technologies (IDT). The heteroduplex substrate was prepared by annealing with 2 μM 3′-FAM–labeled RNA and 4 μM 5′-TAMRA–labeled DNA. A 3′-FAM–labeled ssDNA substrate, with a sequence equivalent to that of the labeled RNA, was also purchased from IDT.

Exonuclease assays of **Figures 5a–c** were performed at 37 °C for 30 min. Reaction mixtures (20 μl volume) contained 30 mM Tris, pH 8.0, 50 mM NH_4Cl, 2 mM $MgCl_2$, 0.5 mM DTT, 25 μg/ml BSA, 5′-end radiolabeled RNA (~100 counts per second) or fluorescently labeled oligonucleotides (2 μM) or heteroduplex and the indicated amount of recombinant Dxo1 (Ydr370C). After the reaction, nucleic acids were isolated by phenol/chloroform extraction and ethanol precipitation and fractionated by PAGE using a gel with 10% or 15% acrylamide and 7 M urea. The radiolabeled RNAs were analyzed by PhosphorImager, and the fluorescently labeled oligonucleotides were visualized on a UV illuminator. Assays were repeated at least three times to ensure reproducibility.

The 5′-end-cap ^{32}P-labeled pcP RNA for **Figure 4** was generated with [α-^{32}P]GTP as described previously[42,43]. The 5′-end ^{32}P-labeled triphosphate RNA and uniformly ^{32}P-labeled capped RNA for **Figure 4b**,**d**,**e** and **Figure 5d**,**e** were transcribed from pcDNA3 polylinker PCR DNA template with T7 RNA polymerase in the presence of [γ-^{32}P]GTP or [α-^{32}P]GTP with or without cap analog in the reaction, respectively . The 5′-monophosphate uniformly ^{32}P-labeled RNAs were generated by methyl-capped uniformly ^{32}P-labeled RNA digested with human Dcp2 decapping enzyme to generate the 5′-end monophosphate RNA. RNA lacking a phosphate at the 5′ end was generated by treating uniformly ^{32}P-labeled triphosphate RNA with calf intestinal alkaline phosphatase (CIP).

The *in vitro* decay assays were carried out as described[15] with the indicated His-tagged recombinant proteins at 37 °C. The RNA decay products were resolved by 8% denaturing PAGE or polyethyleneimine-cellulose TLC (PEI-TLC) plates developed in 0.45 M $(NH_4)_2SO_4$, 0.7 M KH_2PO_4 or 1 M $(NH_4)_2SO_4$, as indicated, at room temperature. Dried gels or TLC plates were exposed to a phosphor screen and detected by a Molecular Dynamics PhosphorImager (Storm860) and quantitated with ImageQuant software.

Real-time PCR. Yeast total RNAs were reverse transcribed into cDNAs with M-MLV reverse transcriptase and random primers (Promega). The real-time reverse-transcription PCR was carried out on Rotor-Gene 3000 (Corbett Research) with iTaq SYBR Green Supermix with ROX kit (Bio-Rad). CYH2, PGK1, ACT1 and 18S rRNA primer pairs are listed in **Supplementary Table 3**.

Cap antibody immunoprecipitation. Methyl-capped RNA immunoprecipitation (IP) was carried out with 15 μl agarose-conjugated anti-2,2,7-trimethylguanosine antibody (Calbiochem, NA02A) in 100 μl buffer as previously described[15] with modifications. Yeast total RNA (0.5 μg) was immunoprecipitated with 15 μl agarose-conjugated anti-2,2,7-trimethylguanosine antibody beads in 100 μl buffer containing 1× PBS, 0.025% NP-40, 1 unit/μl rRNasin RNase inhibitor (Promega) and incubated at room temperature for 1 h. The beads were centrifuged at 300*g* for 20 s, and the supernatant, containing unbound incompletely capped mRNAs, was collected. The beads were washed three times at room temperature for 10 min with 1× PBS containing 300 mM NaCl and 0.05% NP-40. The wash solutions were pooled with the supernatant and precipitated to collect the unbound incompletely capped mRNA fraction. Methyl-capped mRNAs were eluted from the beads with RNA elution buffer (7 M U rea, 2% SDS, 0.35 M NaCl, 10 mM EDTA, 10 mM Tris, pH 7.5) by incubating at 65 °C for 3 min. The isolated methyl-capped mRNAs and incompletely capped mRNAs were reverse transcribed into cDNA with random primers and M-MLV reverse transcriptase (Promega) and quantified by real-time quantitative PCR normalized relative to the input 0.5 μg yeast total RNA. 18S rRNA was used to normalize the RNA input.

33. Doublié, S. *et al.* Crystallization and preliminary X-ray analysis of the 9 kDa protein of the mouse signal recognition particle and the selenomethionyl-SRP9. *FEBS Lett.* **384**, 219–221 (1996).
34. Otwinowski, Z. & Minor, W. Processing of X-ray diffraction data collected in oscillation mode. *Methods Enzymol.* **276**, 307–326 (1997).

doi:10.1038/nsmb.2381

35. Weeks, C.M. & Miller, R. The design and implementation of SnB v2.0. *J. Appl. Crystallogr.* **32**, 120–124 (1999).
36. Terwilliger, T.C. SOLVE and RESOLVE: automated structure solution and density modification. *Methods Enzymol.* **374**, 22–37 (2003).
37. Jones, T.A., Zou, J.Y., Cowan, S.W. & Kjeldgaard, M. Improved methods for building protein models in electron density maps and the location of errors in these models. *Acta Crystallogr. A* **47**, 110–119 (1991).
38. Emsley, P. & Cowtan, K.D. Coot: model-building tools for molecular graphics. *Acta Crystallogr. D Biol. Crystallogr.* **60**, 2126–2132 (2004).
39. Brünger, A.T. *et al.* Crystallography & NMR System: a new software suite for macromolecular structure determination. *Acta Crystallogr. D Biol. Crystallogr.* **54**, 905–921 (1998).
40. Schwer, B., Saha, N., Mao, X., Chen, H.W. & Shuman, S. Structure-function analysis of yeast mRNA cap methyltransferase and high-copy suppression of conditional mutants by AdoMet synthase and the ubiquitin conjugating enzyme Cdc34p. *Genetics* **155**, 1561–1576 (2000).
41. Köhrer, K. & Domdey, H. Preparation of high molecular weight RNA. *Methods Enzymol.* **194**, 398–405 (1991).
42. Wang, Z., Day, N., Trifillis, P. & Kiledjian, M. An mRNA stability complex functions with poly(A)-binding protein to stabilize mRNA *in vitro*. *Mol. Cell. Biol.* **19**, 4552–4560 (1999).
43. Wang, Z., Jiao, X., Carr-Schmid, A. & Kiledjian, M. The hDcp2 protein is a mammalian mRNA decapping enzyme. *Proc. Natl. Acad. Sci. USA* **99**, 12663–12668 (2002).